Free-Carrier-Induced Ferroelectricity in Layered Perovskites

Shutong Li and Turan Birol*
Department of Chemical Engineering and Materials Science, University of Minnesota, Minneapolis, Minnesota 55455, USA

(Received 5 March 2021; accepted 19 July 2021; published 18 August 2021)

Doping ferroelectrics with carriers is often detrimental to polarization. This makes the design and discovery of metals that undergo a ferroelectriclike transition challenging. In this Letter, we show from first principles that the oxygen octahedral rotations in perovskites are often enhanced by electron doping, and this can be used as a means to strengthen the structural polarization in certain hybrid-improper ferroelectrics—compounds in which the polarization is not stabilized by the long-range Coulomb interactions but is instead induced by a trilinear coupling to octahedral rotations. We use this design strategy to predict a cation ordered Ruddlesden-Popper compound that can be driven into a metallic ferroelectriclike phase via electrolyte gating.

DOI: 10.1103/PhysRevLett.127.087601

Ferroelectrics, insulators with a spontaneous and switchable electric polarization, are promising for a wide range of applications and pose a number of fundamental questions [1–4]. While ferroelectricity is observed in a wide range of material classes and can be driven by a variety of mechanisms, the most studied ferroelectrics are transition metal oxides, such as $BaTiO_3$, where the emergence of a polar order parameter is due to a crystal structural distortion driven by the interatomic hybridization and long-range Coulomb interactions [5,6]. Because of the role of the long-range interactions in driving the polar structural distortion, introduction of free charge carriers to ferroelectrics not only screens the ferroelectric polarization, but it also suppresses the structural distortion often [7].

While "structurally polar metals" (metals with a polar point group) are rather common, "ferroelectric metals" (metals that undergo a phase transition from a centrosymmetric to a polar crystal structure [8]) are rather rare. It took almost 50 years after the possibility of a ferroelectriclike transition in a metal was first raised [9] for the unambiguous experimental observation of such a transition in $LiOsO_3$ [10]. The first observation of polarization switching in a ferroelectric (semi)metal is even more recent [11,12]. The interest in polar and ferroelectriclike metals is continuing to increase in both bulk and heterostructures [13–24], and they continue to promise both a fertile playground for interesting emergent phenomena (including, but not limited to, mixed singlet-triplet superconductivity [25] and novel optical effects [26]) and immediate relevance to applications as polar electrodes [27].

Emergence of polarization in $(Sr, Ca)Ru_2O_6$, $Ca_3Ru_2O_7$, and ultrathin $NdNiO_3$ films has been studied in detail [28–30], and it was shown that the polarization in these materials is robust against metallicity because the polar displacements are driven by their coupling to zone-boundary phonon modes and are mainly decoupled with the electrons around the Fermi level. "Metallized ferroelectrics" (insulating ferroelectrics that are doped to introduce charge carriers) are also studied intensively, and the effects of free carriers on the polarization and polar instabilities have been analyzed recently, introducing ideas such as metascreening [31] and elucidating the trends in the second-order Jahn-Teller effect under carrier doping [32]. Barring a volume expansion, the most common effect of charge doping in proper ferroelectrics is the suppression of the ferroelectric polarization; for example, ~0.11 electrons per formula unit is sufficient to completely suppress the polarization in $BaTiO_3$ and render it centrosymmetric [7,33,34].

In this Letter, we show that a particular group of ferroelectrics, the $A_3Sn_2O_7$ hybrid-improper ferroelectrics (HIFs) [35–39] behave differently, and their structural polarization is strongly enhanced by the free electrons introduced by chemical doping or electrostatic gating. This is related to an increase in the oxygen octahedral rotation angles induced by the added electrons in the parent perovskite compounds, which in turn leads to a larger structural polarization in these layered perovskite Ruddlesden-Popper (RP) phases [40]. We also show that it is possible to exploit this mechanism to obtain free-carrier-induced polarization, in other words, design a material that develops a ferroelectriclike structural instability when free electrons are introduced via, for example, electrostatic or electrolyte gating.

Oxygen octahedral rotations in perovskites.—We start by reviewing the symmetry and octahedral rotations in ABO_3 perovskites. Most perovskite oxides have the orthorhombic space group of *Pnma* at low temperature [41]. The atomic displacements that lead to the *Pnma* symmetry can be expanded in terms of the irreducible representations (irrep) of the reference space group $Pm\bar{3}m$ [42,43]. The *Pnma* structure has multiple nonzero strains (Γ_1^+, Γ_3^+, Γ_5^+) and atomic displacements (R_4^-, R_5^-, X_5^-, M_2^+, and M_3^+). Most of these distortions are "secondary": they are nonzero

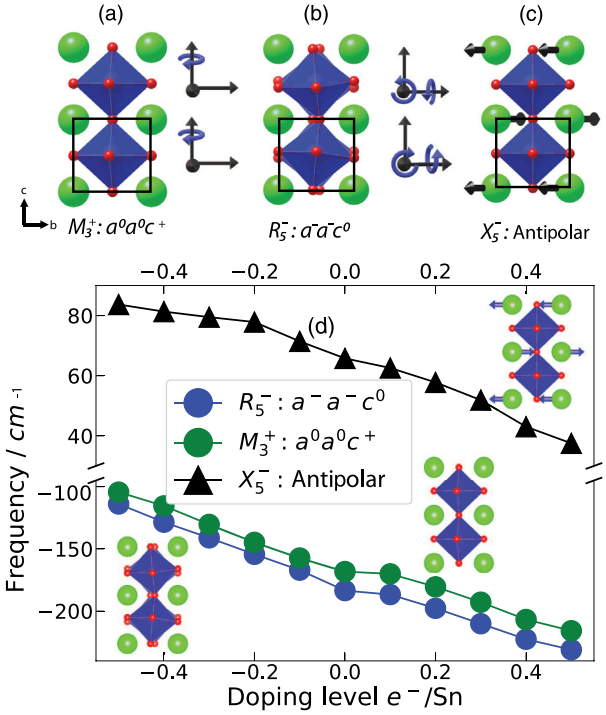

FIG. 1. (a)–(c)The three normal modes in Eq. (1) that are relevant to the *Pnma* phase of perovskites. (d) The phonon frequencies of cubic ($Pm\bar{3}m$) $SrSnO_3$ under doping and fixed volume. The green and red spheres represent the *A* site and oxygen ions, respectively, and the *B*-site atoms are in the center of the blue octahedra. (a) In-phase rotation around the *c* axis ($a^0a^0c^+$ in Glazer notation). (b) Out-of-phase rotation around the *ab* axis $a^-a^-c^0$. (c) The antipolar displacement in the *ab* plane, where the irrep direction is $X_5^-(a,a;0,0;0,0)$. With increasing number of electrons, the unstable rotation modes get more unstable, and the antipolar X_5^- mode gets softened (but remains stable).

only because of couplings with other, "primary" distortions. The *Pnma* structure can be obtained by a combination of only two primary irreps (R_5^- and M_3^+), which correspond to the out-of-phase and in-phase oxygen octahedral rotations shown in Figs. 1(a) and 1(b) [44]. Both of these space irreps are three-dimensional, where the three orthogonal directions correspond to octahedral rotations around the three cubic axes. The phonons corresponding to both of these octahedral rotations are unstable in the cubic reference structure of *Pnma* perovskites. The *Pnma* structure ($a^-a^-c^+$ in the Glazer notation) has out-of-phase rotations around [110] and in-phase rotations around [001], which is equivalent to order parameter directions $R_5^-(a,a,0)$ and $M_3^+(0,0,a)$. These two modes, which we henceforth refer to as *R* and *M* for brevity, couple with the $X_5^-(a,a;0,0;0,0)$ mode (referred to as *X* for brevity) at the trilinear order. Hence, the Landau free energy up to third order is

$$\mathcal{F} = \alpha_R R^2 + \alpha_M M^2 + \alpha_X X^2 + \gamma RMX. \qquad (1)$$

The *X* mode corresponds to an out-of-phase displacement of the *A*-site cations as showed in Fig. 1(c) and is typically stable, but it has a nonzero amplitude $X = \gamma RM/2\alpha$ in the low temperature structure. *X* can be referred to as a "hybrid-improper" order parameter, because it is induced in the ground state by a combination of two primary order parameters.

In heterostructures where translational symmetry is broken by layered cation ordering, or in layered perovskites (RPs), modes that give rise to transverse out-of-phase displacements of the *A* site (related to the X_5^- in perovskites) attain a polar character and are responsible for the hybrid-improper ferroelectricity [35,45,46]. For this reason, understanding the behavior of this mode in bulk perovskites is essential for understanding the polarization trends in HIFs. As an example *Pnma* perovskite system, we consider $SrSnO_3$. While $SrSnO_3$ is orthorhombic at room temperature, its Goldschmidt tolerance factor $t = [(R_{Sr} + R_O)/\sqrt{2}(R_{Sn} + R_O)] = 0.96$ is close enough to 1 so that it undergoes a series of phase transitions to the cubic phase above 1295 K and its structural ground state can be modified by biaxial strain [47,48]. In Fig. 1(d), we show the phonon frequencies for the *R*, *M*, and *X* modes as a function of doping from first principles density-functional theory (DFT) calculations. (The technical details of the calculations are discussed in the Supplemental Material [49].) The phonon frequencies are proportional to the square root of the α coefficients in Eq. (1) and can be used to study the instabilities. Unstable modes have imaginary frequencies, which are plotted as negative numbers. We simulate the effect of free carriers in this nominally insulating compound by changing the total number of electrons in the calculation, while keeping the system neutral by adding a homogeneous background charge. Unlike chemical substitution, this approach does not introduce any steric differences or disorder into the system. In this respect, it is a better representation of electrostatic or electrolyte gated systems rather than chemical doping. We consider a wide range of carrier doping up to 0.5 electrons per Sn atom, which is larger than the typical concentrations experimentally achievable [64]. We keep the unit cell volume fixed in order to separate out the volume expansion effects. The volume expansion does not modify the trends we report significantly [49].

The results in Fig. 1(d) show that both the rotation modes R_5^- and M_3^+, which have imaginary frequencies in the undoped compound, become more unstable with the introduction of free electrons, in other words, α_R and α_M become more negative with added electrons. Similarly, the frequency of the stable X_5^- mode decreases with increasing electron concentration, and so α_X becomes smaller. The trilinear coupling γ does not change significantly under doping, and the changes in the higher-order coefficients are qualitatively insignificant [49]. As a result, the softening of X_5^- and the strengthening of the R_5^- and M_3^+ instabilities

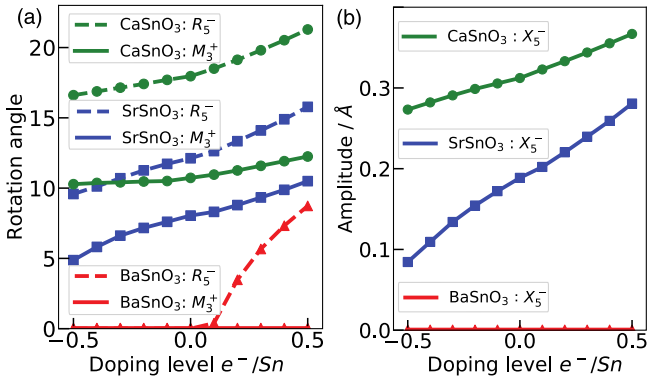

FIG. 2. Results of DFT structure optimizations under fixed volume. Both (a) the octahedral rotation angles and (b) the antipolar mode amplitudes increase with increasing number of electrons, as expected from the phonon frequencies in Fig. 1(d).

under electron doping lead to larger rotation angles and antipolar amplitudes as shown in Fig. 2. This trend is observed not only in *Pnma* perovskites $SrSnO_3$ and $CaSnO_3$, but also in cubic perovskites like $BaZrO_3$, which develops a R_5^- instability when electron doped [49]. A similar enhancement of octahedral rotations was predicted by DFT in $SmNiO_3$ [65] and both DFT and x-ray diffraction points to enhanced octahedral rotations in photodoped $EuTiO_3$ [66].

This effect of carriers on octahedral rotations can be explained by considering the densities of states. The valence bands in stannates consist of oxygen-p bands, whereas the conduction band is formed by Sn-s [67]. The added electrons fill states with Sn-s character, and the valence of Sn^{4+} becomes $Sn^{+4-\delta}$. This decreases the Sn-O electrostatic attraction, decreases the Sn-O hybridization, and increases the ionic radius of Sn. This reduces the tolerance factor t. Added holes, on the other hand, occupy the O^{2-} anions and make them $O^{-2+\delta}$. This reduces the attraction between the A site cation (Ba, Sr, or Ca) and oxygens, which is the driving force of rotational instabilities. Hence, rotation modes become less unstable.

Hybrid-improper ferroelectrics.—We now move on to $A_3B_2O_7$ HIFs and consider $Sr_3Sn_2O_7$ as an example. $Sr_3Sn_2O_7$ is an $n = 2$ RP compound, which can be considered as a layered perovskite with an extra SrO layer after every pair of $SrSnO_3$ bilayers. It is experimentally verified to be a ferroelectric [36,37], and its polarization is induced through the hybrid-improper mechanism, which involves the trilinear coupling between the polar mode (Γ_5^-, which we denote as P) and two octahedral rotation modes (X_3^- and X_2^+, which we denote as Q_1 and Q_2) shown in Fig. 3(a). These modes are the counterparts of the antipolar A-site displacement X_5^- mode and the octahedral rotation modes R_5^- and M_3^+ in bulk perovskites. Two crucial differences between the $A_3B_2O_7$ RP and the ABO_3 perovskite structures are (i) in the smaller Brillouin zone of the RP structure, both the octahedral rotation modes Q_1

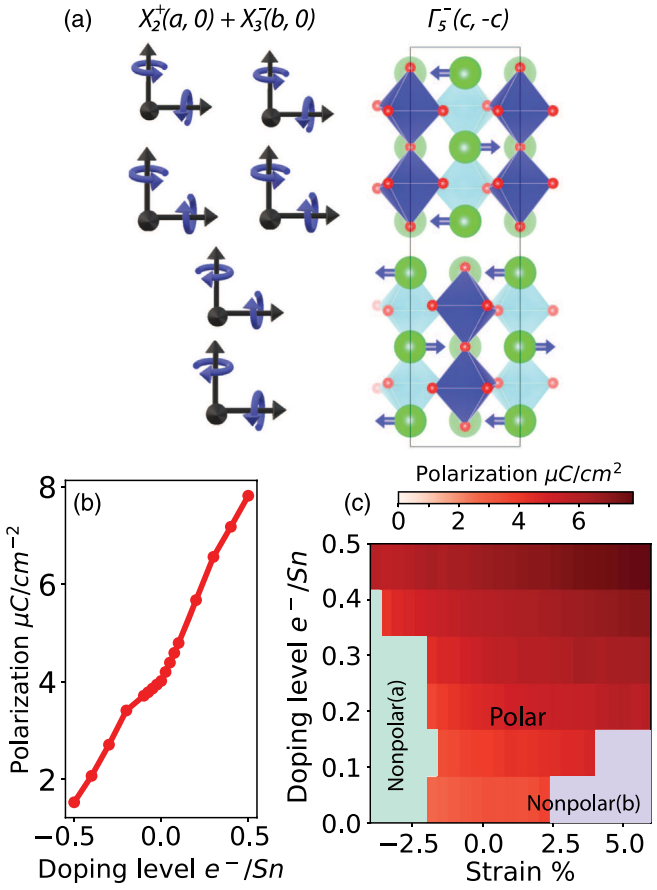

FIG. 3. (a) The structure of $Sr_3Sn_2O_7$ includes three structural distortion modes with respect reference $I4/mmm$ structure: Two oxygen octahedral rotation modes (X_2^+ and X_3^-) and a polar mode (Γ_5^-). (b) The structural polarization strength of $Sr_3Sn_2O_7$ as a function of doping level. The structural polarization is as the sum of the products of the nominal charge and polar displacements of ions [49]. (c) The doping-strain phase diagram of $Sr_3Sn_2O_7$. The nonpolar(a) and nonpolar(b) phases have $Aeaa$ and $P4_2/mnm$ space groups, respectively [49].

and Q_2 have the same wave vector, and hence can couple to zone center modes at the trilinear order, and (ii) the out-of-phase A-site displacement is now a polar Γ mode because the dipole moments induced by the symmetry inequivalent A sites do not cancel. The shortest free energy that explains the polarization up to third order is

$$\mathcal{F} = \alpha_1 Q_1^2 + \alpha_2 Q_2^2 + \alpha_P P^2 + \gamma Q_1 Q_2 P. \qquad (2)$$

The trilinear coupling γ between the unstable Q_1 and Q_2 rotations with $\alpha_{1,2} < 0$ and the stable polar mode P with $\alpha_P > 0$ gives rise to a nonzero polarization $P = \gamma Q_1 Q_2 / 2\alpha_P$ in the ground state.

In order to elucidate the change in the structural polarization in $Sr_3Sn_2O_7$ when free carriers are introduced, we optimize the crystal structure again with different numbers of added electrons or holes. The results in

Fig. 3(b) show that added electrons increase the polarization, similar to the increased antipolar X mode amplitude in $SrSnO_3$. This can be explained by the fact that the mechanism that leads to enhancement of octahedral rotations in the electron doped $SrSnO_3$ is essentially a local mechanism that also applies to $Sr_3Sn_2O_7$, which also has a similar DOS with Sn-s bands on the conduction band. Filling the conduction band increases the effective ionic radius of the Sn ions, which in turn increases the amplitude of Q_1 and Q_2 octahedral rotations and hence enhances the polarization P. In the HIF $Ca_3Ru_2O_7$ or the proper geometric ferroelectriclike $LiOsO_3$, the polarization is persistent against free carriers because of the absence of significant coupling between the electronic states near the Fermi level and the unstable phonons [28,68]. In $Sr_3Sn_2O_7$, there is a strong effect of the conduction band occupation on the lattice instabilities, which is not reported in these other metallic ferroelectriclike compounds.

The enhanced rotations also expand the biaxial strain range where $Sr_3Sn_2O_7$ is structurally polar. In Fig. 3(c), we show the strain-doping phase diagram of $Sr_3Sn_2O_7$, calculated by fixing the in-plane lattice parameters and relaxing the out-of-plane one to simulate the boundary conditions on a thin film lattice matched to a substrate. Insulating, undoped $Sr_3Sn_2O_7$ is known to undergo a transition to a nonpolar phase above $\sim \mp 2\%$ biaxial strain [50] like many other compounds [69]. Figure 3(c) shows that not only doping enhances polarization at fixed volume, but it also stabilizes the polar phase at wider strain ranges. The polar-nonpolar transition induced by epitaxial strain is driven by the disappearance of one of two rotation modes in the polar phase [50]. The free electrons increase the stability of both rotation modes, which make this phase transition occur at a higher strain value.

Ferroelectriclike transition induced by free electrons.—The strong effect of free electrons on stabilizing a metallic ferroelectriclike phase in $Sr_3Sn_2O_7$ leads to the question of whether it is possible to drive a centrosymmetric compound to a polar phase by doping it with free electrons without the help of biaxial strain. We scanned a number of $A_3B_2O_7$ oxides, but could not find an example that undergoes a polar phase transition for dopings up to 0.5 e^- per B-site cation, which is already beyond what is experimentally achievable via methods such as electrostatic gating. In order to design a material that is closer to a structural phase transition than $Sr_3Sn_2O_7$, we turn to "targeted chemical pressure," which involves selectively substituting part of Sr ions with larger Ba cations [70]. While it is not always possible to order same charge cations in bulk, molecular beam epitaxy has been successfully used to obtain targeted chemical pressure in other RP phases $(SrTiO_3)_n(BaTiO_3)_mSrO$ [70]. In $Sr_3Sn_2O_7$ ceramics, up to 10% of Ba ions are reported to preferentially substitute inequivalent Sr sites, however, the ordering tendencies depend sensitively on changes in the substitution amount [39]. We consider a structure where the 2/3 of Sr cations are substituted with Ba to form $Ba_2SrSn_2O_7$, where the Ba cations are on the double-rocksalt layers of the RP structure, as shown in Fig. 4(a). While this structure is not energetically the most stable one [49], it may in principle be synthesized via layer-by-layer growth. The lowest energy structure of $Ba_2SrSn_2O_7$ is centrosymmetric when undoped and strain relaxed, but introducing electrons to the conduction band leads to a transition to a polar structure with space group $Cmc2_1$ [Fig. 4(b)]. Thus, $Ba_2SrSn_2O_7$ is a free-carrier-induced metallic ferroelectric. Like in undoped $A_3B_2O_7$ compounds, biaxial strain also modifies the stability range of the polar phase of $Ba_2SrSn_2O_7$.

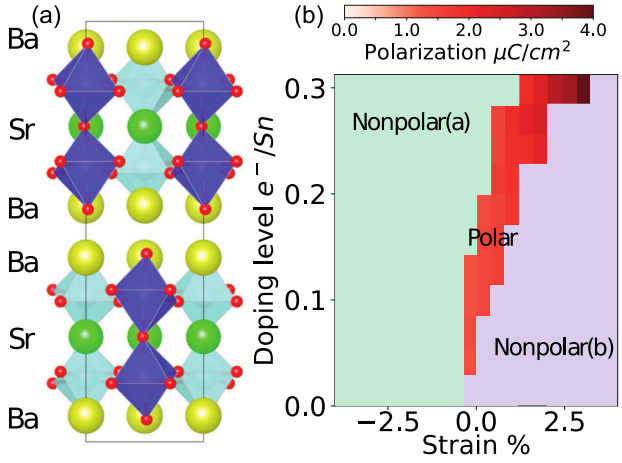

FIG. 4. (a) The structure and (b) a doping-strain phase diagram of $Ba_2SrSn_2O_7$. Yellow spheres represent Ba atoms. The nonpolar(a) and nonpolar(b) phases have $Aeaa$ and $P4_2/mnm$ symmetries, respectively.

Experimental verification of this prediction is possible. $Ba_3Sn_2O_7$ is stable in bulk [71], and thin films of both Sr and Ba stannate perovskites were grown by multiple groups [48,72,73]. If the free charge is constrained in the top $\sim$10 Å of a $Ba_2SrSn_2O_7$ film, the charge density needed to stabilize the polar phase is $\sim 5 \times 10^{13}$ cm^{-2}. Dielectric based gating allows densities of $\sim 10^{13}$ cm^{-2} [74], and it is possible to obtain densities exceeding $\sim 10^{14}$ cm^{-2} via ionic liquid gating [64,75,76]. Thus, it is possible to induce in-plane structural polarization using electrolyte gating. The polarization can be observed by second harmonic generation, as was done in $LiOsO_3$ [77].

Other $A_3B_2O_7$ *compounds.*—This mechanism is very general, and it could be expected to be applicable to many other HIF oxides. However, our calculations on $Ca_3Ti_2O_7$ and $Sr_3Zr_2O_7$, which we discuss in the Supplemental Material [49], indicate that this is not the case. Even though the parent $CaTiO_3$ and $SrZrO_3$ compounds behave very similar to $SrSnO_3$ under doping, the structural polarization of both $Ca_3Ti_2O_7$ and $Sr_3Zr_2O_7$ decrease upon electron doping. The reason is a subtle difference in the nature of polarization in these compounds: While both $Ca_3Ti_2O_7$ and $Sr_3Zr_2O_7$ have HIF ground states, in their

$I4/mmm$ reference structure they also display weak polar Γ point instabilities [51,52]. As a result of this instability, $Ca_3Ti_2O_7$ has a significant Ti contribution to polarization. This contribution is reduced as electrons are introduced to the system, because free carriers suppress the Ti-O hybridization and harden this soft mode in $Ca_3Ti_2O_7$ as they do in titanate perovskites $CaTiO_3$ or $BaTiO_3$ [7,8,49]. $Sr_3Sn_2O_7$, on the other hand, has no Γ instabilities and has only a negligible SnO_2 layer polarization. This suggests the stannate perovskites as a unique group of compounds that can display free-carrier-enhanced (or induced) hybrid-improper ferroelectricity.

Summary.—Using first principles calculations and studying the oxygen octahedral rotations in *Pnma* perovskites under doping, we showed that the structural polarization in stannate HIFs is not only robust against free carriers, but it is also enhanced. We furthermore predicted a yet-to-be-synthesized compound $Ba_2SrSn_2O_7$ that undergoes a centrosymmetric to polar transition under electron concentrations that are experimentally achievable by ionic liquid or gel gating. While our calculations are strictly at zero temperature and finding temperature dependence of lattice distortions requires molecular dynamics or effective Hamiltonian studies, the large energy gains we find suggest the possibility of observing this effect even at room temperature [49]. Our results show that the improper ferroelectricity driven by steric lattice instabilities can serve as a means to obtain carrier-induced ferroelectricity in compounds where those instabilities are strengthened by the free carriers.

The data and metadata for the first principles calculations reported in this study are available in the Data Repository of the University of Minnesota (DRUM), and can be accessed at [78].

We acknowledge helpful suggestions of an anonymous referee for the discussion about $Ca_3Ti_2O_7$. This work was supported primarily by the National Science Foundation through the University of Minnesota MRSEC under Grant No. DMR-2011401. We acknowledge the Minnesota Supercomputing Institute (MSI) at the University of Minnesota for providing resources that contributed to the research results reported within this Letter.

*tbirol@umn.edu

[1] J. Dai, in *Ferroic Materials for Smart Systems* (Wiley, New York, 2020), pp. 15–46.
[2] K. M. Rabe and P. Ghosez, Top. Appl. Phys. **105**, 117 (2007).
[3] L. W. Martin and A. M. Rappe, Nat. Rev. Mater. **2**, 16087 (2017).
[4] J. F. Scott, Science **315**, 954 (2007).
[5] P. Ghosez, X. Gonze, and J. P. Michenaud, Europhys. Lett. **33**, 713 (1996).
[6] R. E. Cohen, Nature (London) **358**, 136 (1992).
[7] Y. Wang, X. Liu, J. D. Burton, S. S. Jaswal, and E. Y. Tsymbal, Phys. Rev. Lett. **109**, 247601 (2012).
[8] N. A. Benedek and T. Birol, J. Mater. Chem. C **4**, 4000 (2016).
[9] P. W. Anderson and E. I. Blount, Phys. Rev. Lett. **14**, 217 (1965).
[10] Y. Shi, Y. Guo, X. Wang, A. J. Princep, D. Khalyavin, P. Manuel, Y. Michiue, A. Sato, K. Tsuda, S. Yu, M. Arai, Y. Shirako, M. Akaogi, N. Wang, K. Yamaura, and A. T. Boothroyd, Nat. Mater. **12**, 1024 (2013).
[11] Z. Fei, W. Zhao, T. A. Palomaki, B. Sun, M. K. Miller, Z. Zhao, J. Yan, X. Xu, and D. H. Cobden, Nature (London) **560**, 336 (2018).
[12] P. Sharma, F.-X. Xiang, D.-F. Shao, D. Zhang, E. Y. Tsymbal, A. R. Hamilton, and J. Seidel, Sci. Adv. **5**, eaax5080 (2019).
[13] M. Meng, Z. Wang, A. Fathima, S. Ghosh, M. Saghayezhian, J. Taylor, R. Jin, Y. Zhu, S. T. Pantelides, J. Zhang, E. W. Plummer, and H. Guo, Nat. Commun. **10**, 1 (2019).
[14] H. J. Xiang, Phys. Rev. B **90**, 094108 (2014).
[15] I. Lo Vecchio, G. Giovannetti, M. Autore, P. Di Pietro, A. Perucchi, J. He, K. Yamaura, M. Capone, and S. Lupi, Phys. Rev. B **93**, 161113(R) (2016).
[16] H. M. Liu, Y. P. Du, Y. L. Xie, J. M. Liu, C. G. Duan, and X. Wan, Phys. Rev. B **91**, 064104 (2015).
[17] A. Narayan, J. Phys. Condens. Matter **32**, 125501 (2020).
[18] Y. R. Wang, S. Wang, H. L. Tao, Y. Cui, S. M. Liu, M. He, B. Song, and Z. H. Zhang, Solid State Commun. **323**, 114099 (2021).
[19] F. Jin, L. Wang, A. Zhang, J. Ji, Y. Shi, X. Wang, R. Yu, J. Zhang, E. W. Plummer, and Q. Zhang, Proc. Natl. Acad. Sci. U.S.A. **116**, 20322 (2019).
[20] J.-Y. Shan, A. de la Torre, N. J. Laurita, L. Zhao, C. D. Dashwood, D. Puggioni, C. X. Wang, K. Yamaura, Y. Shi, J. M. Rondinelli, and D. Hsieh, Phys. Rev. Research **2**, 033174 (2020).
[21] Z. Yimer and H. Fu, Phys. Rev. B **101**, 174105 (2020).
[22] S. Ghosh, A. Y. Borisevich, and S. T. Pantelides, Phys. Rev. Lett. **119**, 177603 (2017).
[23] A. Zabalo and M. Stengel, Phys. Rev. Lett. **126**, 127601 (2021).
[24] R. C. Xiao, D. F. Shao, W. Huang, and H. Jiang, Phys. Rev. B **102**, 024109 (2020).
[25] S. Salmani-Rezaie, K. Ahadi, and S. Stemmer, Nano Lett. **20**, 6542 (2020).
[26] V. P. Mineev and Y. Yoshioka, Phys. Rev. B **81**, 094525 (2010).
[27] D. Puggioni, G. Giovannetti, and J. M. Rondinelli, J. Appl. Phys. **124**, 174102 (2018).
[28] D. Puggioni and J. M. Rondinelli, Nat. Commun. **5**, 3432 (2014).
[29] T. H. Kim, D. Puggioni, Y. Yuan, L. Xie, H. Zhou, N. Campbell, P. J. Ryan, Y. Choi, J. W. Kim, J. R. Patzner, S. Ryu, J. P. Podkaminer, J. Irwin, Y. Ma, C. J. Fennie, M. S. Rzchowski, X. Q. Pan, V. Gopalan, J. M. Rondinelli, and C. B. Eom, Nature (London) **533**, 68 (2016).
[30] S. Lei, M. Gu, D. Puggioni, G. Stone, J. Peng, J. Ge, Y. Wang, B. Wang, Y. Yuan, K. Wang, Z. Mao, J. M. Rondinelli, and V. Gopalan, Nano Lett. **18**, 3088 (2018).

[31] H. J. Zhao, A. Filippetti, C. Escorihuela-Sayalero, P. Delugas, E. Canadell, L. Bellaiche, V. Fiorentini, and J. Íñiguez, Phys. Rev. B **97**, 054107 (2018).

[32] D. Hickox-Young, D. Puggioni, and J. M. Rondinelli, Phys. Rev. B **102**, 014108 (2020).

[33] T. Kolodiazhnyi, M. Tachibana, H. Kawaji, J. Hwang, and E. Takayama-Muromachi, Phys. Rev. Lett. **104**, 147602 (2010).

[34] C. Xia, Y. Chen, and H. Chen, Phys. Rev. Mater. **3**, 054405 (2019).

[35] N. A. Benedek and C. J. Fennie, Phys. Rev. Lett. **106**, 107204 (2011).

[36] Y. Wang, F. T. Huang, X. Luo, B. Gao, and S. W. Cheong, Adv. Mater. **29**, 1601288 (2017).

[37] S. Yoshida, H. Akamatsu, R. Tsuji, O. Hernandez, H. Padmanabhan, A. Sen Gupta, A. S. Gibbs, K. Mibu, S. Murai, J. M. Rondinelli, V. Gopalan, K. Tanaka, and K. Fujita, J. Am. Chem. Soc. **140**, 15690 (2018).

[38] J. J. Lu, X. Q. Liu, X. Ma, M. S. Fu, A. Yuan, Y. J. Wu, and X. M. Chen, J. Appl. Phys. **125**, 044101 (2019).

[39] B. H. Chen, T. L. Sun, X. Q. Liu, X. L. Zhu, H. Tian, and X. M. Chen, Appl. Phys. Lett. **116**, 042903 (2020).

[40] S. N. Ruddlesden and P. Popper, Acta Crystallogr. **11**, 54 (1958).

[41] M. W. Lufaso and P. M. Woodward, Acta Crystallogr. Sect. B **57**, 725 (2001).

[42] M. I. Aroyo and J. M. Perez-Mato, Acta Crystallogr. Sect. A **54**, 19 (1998).

[43] B. J. Campbell, H. T. Stokes, D. E. Tanner, and D. M. Hatch, J. Appl. Crystallogr. **39**, 607 (2006).

[44] P. M. Woodward, Acta Crystallogr. Sect. B **53**, 32 (1997).

[45] N. A. Benedek, J. M. Rondinelli, H. Djani, P. Ghosez, and P. Lightfoot, Dalton Trans. **44**, 10543 (2015).

[46] A. T. Mulder, N. A. Benedek, J. M. Rondinelli, and C. J. Fennie, Adv. Funct. Mater. **23**, 4810 (2013).

[47] M. Glerup, K. S. Knight, and F. W. Poulsen, Mater. Res. Bull. **40**, 507 (2005).

[48] T. Wang, A. Prakash, Y. Dong, T. Truttmann, A. Bucsek, R. James, D. D. Fong, J.-W. Kim, P. J. Ryan, H. Zhou, T. Birol, and B. Jalan, ACS Appl. Mater. Interfaces **10**, 43802 (2018).

[49] See Supplemental Material at http://link.aps.org/supplemental/10.1103/PhysRevLett.127.087601 for methods, results on other compounds, list of possible structural phases of $A_3B_2O_7$ Ruddlesden-Popper phases, further details of the free energy expansion and higher order coefficients, volume effects, effect of electronic smearing, and the energetics of cation order in $Ba_2SrSn_2O_7$, which includes Refs. [7,8,32,50–63].

[50] S. Li and T. Birol, npj Comput. Mater. **6**, 168 (2020).

[51] A. Mulder, Ferroelectricity coupled to octahedral rotations in perovskite oxides from first principles, Ph.D. thesis, Cornell University, 2016.

[52] S. Yoshida, K. Fujita, H. Akamatsu, O. Hernandez, A. Sen Gupta, F. G. Brown, H. Padmanabhan, A. S. Gibbs, T. Kuge, R. Tsuji, S. Murai, J. M. Rondinelli, V. Gopalan, and K. Tanaka, Adv. Funct. Mater. **28**, 1801856 (2018).

[53] P. E. Blöchl, Phys. Rev. B **50**, 17953 (1994).

[54] G. Kresse and D. Joubert, Phys. Rev. B **59**, 1758 (1999).

[55] G. Kresse and J. Hafner, Phys. Rev. B **47**, 558 (1993).

[56] J. P. Perdew, A. Ruzsinszky, G. I. Csonka, O. A. Vydrov, G. E. Scuseria, L. A. Constantin, X. Zhou, and K. Burke, Phys. Rev. Lett. **100**, 136406 (2008).

[57] H. T. Stokes, D. M. Hatch, and B. J. Campbell, Isotropy (2007), http://iso.byu.edu/.

[58] P. Virtanen *et al.*, Nat. Methods **17**, 261 (2020).

[59] A. Filippetti, V. Fiorentini, F. Ricci, P. Delugas, and J. Íñiguez, Nat. Commun. **7**, 11211 (2016).

[60] E. A. Nowadnick and C. J. Fennie, Phys. Rev. B **94**, 104105 (2016).

[61] N. A. Benedek and C. J. Fennie, J. Phys. Chem. C **117**, 13339 (2013).

[62] S. Ivantchev, E. Kroumova, G. Madariaga, J. M. Pérez-Mato, and M. I. Aroyo, J. Appl. Crystallogr. **33**, 1190 (2000).

[63] T. Birol, N. A. Benedek, and C. J. Fennie, Phys. Rev. Lett. **107**, 257602 (2011).

[64] H. Yuan, H. Shimotani, A. Tsukazaki, A. Ohtomo, M. Kawasaki, and Y. Iwasa, Adv. Funct. Mater. **19**, 1046 (2009).

[65] M. Kotiuga and K. M. Rabe, Phys. Rev. Mater. **3**, 115002 (2019).

[66] M. Porer, M. Fechner, M. Kubli, M. J. Neugebauer, S. Parchenko, V. Esposito, A. Narayan, N. A. Spaldin, R. Huber, M. Radovic, E. M. Bothschafter, J. M. Glownia, T. Sato, S. Song, S. L. Johnson, and U. Staub, Phys. Rev. Research **1**, 012005 (2019).

[67] H. Mizoguchi, H. W. Eng, and P. M. Woodward, Inorg. Chem. **43**, 1667 (2004).

[68] N. J. Laurita, A. Ron, J.-Y. Shan, D. Puggioni, N. Z. Koocher, K. Yamaura, Y. Shi, J. M. Rondinelli, and D. Hsieh, Nat. Commun. **10**, 3217 (2019).

[69] X. Z. Lu and J. M. Rondinelli, Nat. Mater. **15**, 951 (2016).

[70] N. M. Dawley, E. J. Marksz, A. M. Hagerstrom, G. H. Olsen, M. E. Holtz, V. Goian, C. Kadlec, J. Zhang, X. Lu, J. A. Drisko, R. Uecker, S. Ganschow, C. J. Long, J. C. Booth, S. Kamba, C. J. Fennie, D. A. Muller, N. D. Orloff, and D. G. Schlom, Nat. Mater. **19**, 176 (2020).

[71] Y. Hinatsu and K. Tezuka, J. Solid State Chem. **138**, 329 (1998).

[72] A. Prakash, J. Dewey, H. Yun, J. S. Jeong, K. A. Mkhoyan, and B. Jalan, J. Vac. Sci. Technol. A **33**, 060608 (2015).

[73] H. Paik, Z. Chen, E. Lochocki, A. Seidner H., A. Verma, N. Tanen, J. Park, M. Uchida, S. Shang, B.-C. Zhou, M. Brützam, R. Uecker, Z.-K. Liu, D. Jena, K. M. Shen, D. A. Muller, and D. G. Schlom, APL Mater. **5**, 116107 (2017).

[74] A. Goldman, Annu. Rev. Mater. Res. **44**, 45 (2014).

[75] S. Z. Bisri, S. Shimizu, M. Nakano, and Y. Iwasa, Adv. Mater. **29**, 1607054 (2017).

[76] C. Leighton, Nat. Mater. **18**, 13 (2019).

[77] H. Padmanabhan, Y. Park, D. Puggioni, Y. Yuan, Y. Cao, L. Gasparov, Y. Shi, J. Chakhalian, J. M. Rondinelli, and V. Gopalan, Appl. Phys. Lett. **113**, 122906 (2018).

[78] https://doi.org/10.13020/wxmc-x946.